J Math Chem (2015) 53:1280–1293
DOI 10.1007/s10910-015-0488-4

ORIGINAL PAPER

Mathematical modeling and simulations on massive hydrogen yield using functionalized nanomaterials

Yue Chan[1]

Received: 6 October 2014 / Accepted: 11 March 2015 / Published online: 19 March 2015

Abstract In this paper, we adopt the mathematical modeling and MD simulation to investigate the possibility of using functionalized nanomaterials, in particular carbon nanotubes and graphene to yield hydrogen from an acidic solution by the mean of reverse osmosis. Positively charged nanomaterials are found to be a necessary condition for such phenomenon to happen. For hydrogen chloride acid under certain external forces, only hydrogen ions could gain sufficient work done to overcome the energy barrier induced by the functionalized nanomaterials, resulting in sole hydrogen ions in the permeate side. Hydrogen could then be produced from hydrogen ions by a chemical reduction. Our numerical results indicate that for the two proposed nanomaterials, functionalized graphene turns out to be the better candidate for the current purpose.

Keywords Mathematical modelling · Continuous approximation · MD simulations · Hydrogen chloride · Ultra-filtration · Functionalized graphene and carbon nanotube · Hydrogen yield

1 Introduction

Hydrogen yield, storage and conversion are key issues in recent hydrogen technology. Unlike other fossil fuels and coals, the combustion of hydrogen with air produces water generating zero carbon emission. Conventional hydrogen production could be achieved by steam reforming, electrolysis and thermolysis. However, they either demand huge energy input or are not environmentally friendly. Recently, several alternative means,

✉ Yue Chan
yue.chan@nottingham.edu.cn

[1] School of Mathematical Sciences, Faculty of Science and Engineering, The University of Nottingham, 199 Taikang East Road, Ningbo 315100, China

in particular biomass are proposed for the hydrogen yield: Demirbas [1] proposes the production of hydrogen from solid wastes using pyrolysis, Zhang et al. [2] investigate the hydrogen yield from an inexpensive and abundant renewable biomass, Tao et al. [3] adopt a two-step process to extract hydrogen from fatty acids in the dark-fermentation of sucrose, Vrije et al. [4] theoretically investigate the hydrogen yield from the glucose fermentation via the EM pathway, Argun et al. [5] investigate the effect of C/N and C/P ratio on the hydrogen yield from the dark fermentation of wheat powder solution. Kumar and Das [6] propose the hydrogen yield using micro-organism and Yu et al. [7] study the extraction of hydrogen from the anaerobic acidogenesis of a high-strength rice winery wastewater mixed with baterial flora. Least but not last, solar energy has also been used for splitting water molecules apart in order to yield hydrogen [8].

In this paper, we are inspired by the present author's previous works on the ultra-filtration using functionalized nanomaterials [9–12] and propose the possibility of hydrogen yield by squeezing an acidic solution, for example HCl through the functionalized nanomaterials, in particular carbon nanotubes and graphene sheets by the mean of reverse osmosis. Functionalization for both materials has already existed. For example, graphene oxide comprises graphene sheets which are decorated by certain functional groups such as hydrophilic oxygen [13], and nanotube rims could be decorated with some functional groups, for example carboxylic groups (–COOH) to sieve cations and anions [14,15]. Recently, numerous computational simulations have been performed on the ultra-filtration using nanomaterials such as nanotubes [14,16–22] and zeolite [23]. All these theoretical studies reveal the speedy and effective ultra-filtration using nanomaterials. However, to the best knowledge of the present author, no article reports on the hydrogen yield using nanomaterials by the mean of reverse osmosis. Reverse Osmosis has been found to possess the merits of low energy consumption and operational costs in comparison to other desalination methods such as multi-stage flash, multi-effect distillation and mechanical vapor compression. Although most theoretical investigations demonstrate the superior filtration performance of such nanomaterials, none of these nanomaterials have successful been proved experimentally for the desalination. Recently, Tanugi and Grossman [24] have nominated nano-porous graphene as a mean for the seawater desalination due to its high mechanical strength and the negligible thickness (See Fig. 1 for details). They claim that graphene possesses the highest water permeability in comparison to all the other existing commercial RO and zeolite [24]. In addition, several experimental investigations have also reported the possibility of producing and transferring a single layered graphene sheet [25], which make this 2D-nano structure more relevant for the desalination at the commercial scale.

However, the simulation approach adopted by Tanugi and Grossman [24] and other computational simulations [14,16–23] have severe temporal and spatial constraints that they are infeasible to take into account ultra-filtration problems in the longer run and larger scale. Here, we adopt the continuous approximation introduced by Cox et al. [26,27] and coarse grain the pairwise interactions among ions, molecules and functional groups so that the time-consuming pairwise calculations could be fasten by evaluating several single or double surface integrals, i.e. Eqs. (2) and (3). The present author has successfully employed such methodology for the seawater desalination using carbon nanotube and functionalized nanotube membranes [9–12], and the ultrafiltration using neutral graphene sheet [28]. Other applications using the present

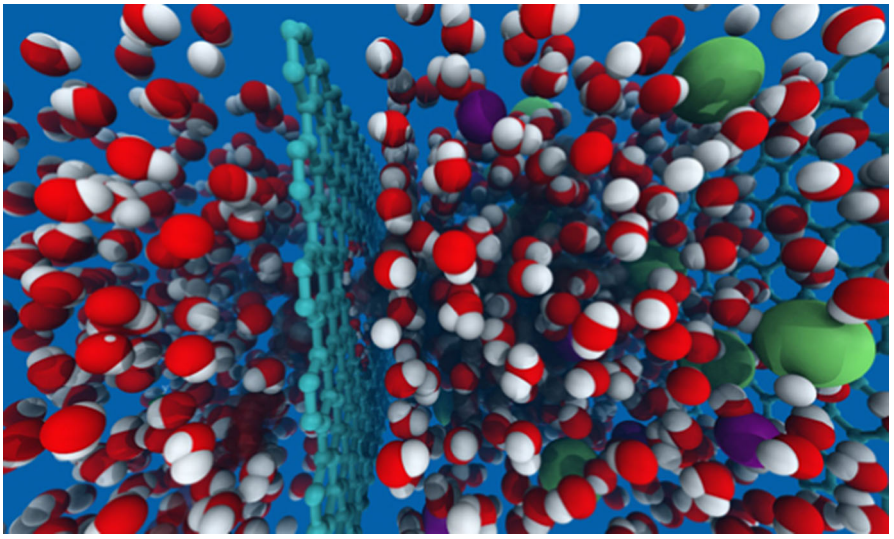

Fig. 1 A computational simulation of desalination using nano-porous graphene, where the *left-hand side* is pure water while the *right-hand side* is salt water (Copyright @MIT)

methodologies include the concentric gold nanoparticles as potential application in drug delivery [29] and the encapsulation of carbon atomic-chains using carbon nanotori and nanotubes [30].

In Sect. 2, we introduce the theoretical and numerical background for the rest of the paper and the corresponding numerical results are presented in Sect. 3. A general conclusion is made in the final section of the paper.

2 Theory and MD simulations

In this section, we provide the theoretical and numerical basis for the rest of the paper. For simplicity, we model the van der Waals forces and the electrostatic interactions between a water molecule or an ion and the functionalized nanomaterials by the usual 6-12 Lennard-Jones potential V [31] and Coulomb's law, respectively which are given by

$$V(\rho_{ij}) = 4\epsilon\left[-\left(\frac{\sigma}{\rho_{ij}}\right)^6 + \left(\frac{\sigma}{\rho_{ij}}\right)^{12}\right] = -\frac{A}{\rho_{ij}^6} + \frac{B}{\rho_{ij}^{12}}, \quad E(\rho_{ij}) = \frac{Q_i Q_j}{\varepsilon \rho_{ij}^2}, \tag{1}$$

where ρ_{ij}, ϵ, σ, Q_i, ε , A and B denote the atomic distance between two typical atoms, the Lennard-Jones potential well depth, the Lennard-Jones distance between two atoms, total charge for i atom, the electrostatic permittivity, the attractive constant and the repulsive constant, respectively. The numerical value of all necessary constants given in this paper is summarized in Table 1.

Table 1 Numerical values for A, B, A_i and B_i as determined by Lorentz–Berthelot mixing rule [38]

Description	Parameter	Value
Radius of water molecule	a	1 Å
Radius of hydrogen ion	a	0.35 Å
Radius of chloride ion	a	1.67 Å
Radius of the graphene pore	b	1.42 Å
Radius of the nanotube pore	b	4 Å
Attractive constant H–C	A_{HC}	6.3 eVÅ^6
Repulsive constant H–C	B_{HC}	5460 eVÅ^{12}
Attractive constant O–C	A_{OC}	17 eVÅ^6
Repulsive constant O–C	B_{OC}	21,600 eVÅ^{12}
Attractive constant Cl–C	A_{ClC}	62.57 eVÅ^6
Repulsive constant Cl–C	B_{ClC}	304,015.33 eVÅ^{12}
Number density of graphene	η_C	0.381 Å^{-2}
Number density of oxygen	η_O	1.274 Å^{-2}
Number density of hydrogen ion	η_H	0.65 Å^{-2}
Number density of chloride ion	η_{Cl}	0.029 Å^{-2}
Angle ϕ	ϕ	0.911 rad

Here, we firstly consider the case of hydrogen chloride solution passing through the functionalized carbon nanotube under an applied force. We employ the basic idea of molecular dynamics simulations which determine the time evolution of the physical system by computing the pairwise interactions between atoms. However, to facilitate rapid computational time, we coarse grain certain atomic interactions among molecules by the continuous approximation [26,27]. We assume that the carbon atoms are smeared across the carbon nanotube which could be approximated as a cylinder, and the oxygen at the water's center, the dissolved hydrogen ion and the dissolved chloride ion are smeared across an envisaged sphere of radius 1, 0.35 and 1.67 Å, respectively so that the van der Waals forces between the oxygen, hydrogen or chloride ions and the nanotube could be approximated by the double surface integral [26,27]. In addition, we assume the hydrogen ion to be a point mass so that the van der Waals forces between the hydrogen on the water molecule and the nanotube are approximated by the single surface integral, where the form of both single and double surface integrals is given by

$$\begin{aligned} F_2^{vdW}(R) &= \eta_1\eta_2 \int \left\{ -\frac{dV(\rho)}{d\rho} \mid_{\perp} \right\} dS_1 dS_2, \\ F_1^{vdW}(R) &= \eta_1 \int \left\{ -\frac{dV(\rho)}{d\rho} \mid_{\perp} \right\} dS_1, \end{aligned} \tag{2}$$

where $\eta_1, \eta_2, -dV(\rho)/d\rho \mid_{\perp}, dS_1$ and dS_2 denote the number density of the nanotube, the number density of the envisaged sphere, the axial force generated by the potential

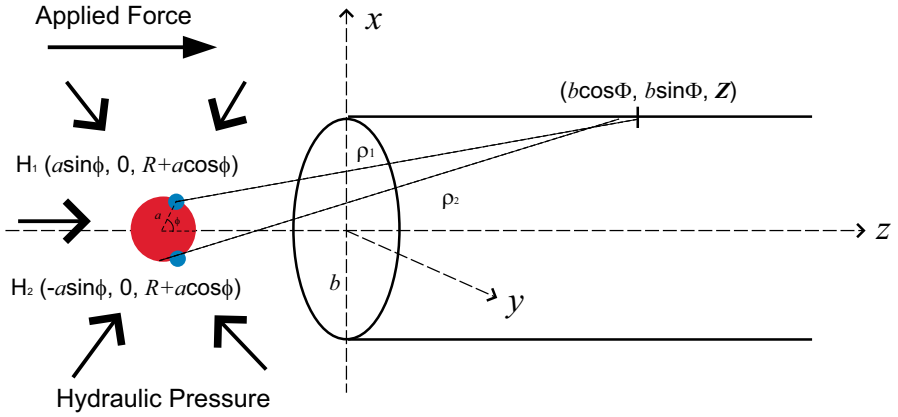

Fig. 2 Kinematics of a water molecule intruding axially into a pore of carbon nanotube, where ρ_1 denotes the atomic distance between a hydrogen atom, H_1 and an arbitrary point on the nanotube and the functional group is assumed to be smeared on the ring of the pore entry. Both the applied and hydraulic forces are shown in terms of *different arrows*

energy given in Eq. (1), the surface element of the nanotube and the surface element of the envisaged sphere, respectively. We comment that the subscripts 1 and 2 under F_1^{vdW} and F_2^{vdW} indicate the single and double surface integrals, respectively. After series of calculations, these integrals end up in certain functions of R, which is an axial distance between the centers of the intruder and the nanotube's pore (See Fig. 2).

To take into account the functionalization of carbon nanotube entries, we assume that the functional group is smeared on the pore vicinity with the length element $\mathrm{d}\ell$ so that the electrostatic forces between the water or the hydrogen and chloride ions and the functional group are given as

$$F_i^e = \int_\ell \frac{q_i \sigma}{\varepsilon \rho_\perp^2} d\ell, \tag{3}$$

where σ denotes the charge density on the functional group. We comment that all the above integrals reduce the multi-body interactions into several two-body interactions and the introduction of the axial forces reduce the 3D problem into the corresponding degenerated 1D problems. According to the prior works performed by the present author [10–12], certain parts of the surface integrals could be solved analytically facilitating rapid computational times.

Since the orientation of water molecules is found to be crucial in this problem [32], we initially fix the configuration of the two hydrogen atoms, which are separated by an angle 2α as shown in Fig. 2 and the possible orientations of the water molecule are generated by two independent angles $\theta \in [0, \pi]$ and $\psi \in [-\pi, \pi]$. Therefore, the distance between the first hydrogen atom (H_1 in Fig. 2) and an arbitrary point on the nanotube, ρ_1 is given by

$$\rho_1^2 = K_1 + K_2 \cos\Phi + K_3 \sin\Phi, \tag{4}$$

where $K_1 = a^2 + b^2 + 2a(R + Z)(\cos\phi\cos\theta - \sin\phi\sin\theta\cos\psi) + (R + Z)^2$, $K_2 = -2ab\sin\theta\sin\psi$ and $K_3 = -2ab(\sin\phi\cos\theta + \cos\phi\sin\theta\cos\psi)$, and where a, b, 2ϕ, R, Z and Φ further denote the radius of the water molecule, the radius of the nanotube, the angle between two hydrogens on the water molecule, the perpendicular distance between the centers of the water molecule and the pore, the Z-axis coordinate system and and the polar angle on the nanotube, respectively (See Fig. 2 for details). Due to the symmetry of two hydrogen atoms, the distance between the second hydrogen and the nanotube could be obtained by replacing ϕ by $-\phi$. We note that the distance between the oxygen or the hydrogen and chloride ions and the nanotube can be deduced in a similar manner. Such atomic distances could then be incorporated into Eqs. (2) and (3) to evaluate F_1^{vdW}, F_2^{vdW} and F_i^e. Since the forces between the hydrogen atoms and the functionalized nanotube are generated by different orientations, the ensemble forces acting on the two hydrogens due to the nanotube on water molecules are determined using the Boltzmann's distribution

$$F_{H_i} = \frac{\sum_j \left\{F_{H_i}(R)_j \exp(-\beta V_{H_i}(R)_j)\right\}}{\sum_j \exp(-\beta V_{H_i}(R)_j)}, \tag{5}$$

where j, $F_{H_i}(R)_j$, β and $V_{H_i}(R)_j$ denote the different orientations, the forces acting on H_i in the j configuration, the reciprocal of the Boltzmann's constant times the temperature, and the potential energy between H_i in the j configuration and the nanotube, respectively. Note that $V_{H_i(R)_j}$ could represent both the van der Waals forces and electrostatic energy, and the temperature effect is thus absorbed in Eq. (5). The total molecular forces between the water molecule in the acidic solution and the functionalized nanotube is therefore written as

$$\begin{aligned} F_W^{tot} &= F_O^{vdW} + F_{H_1}^{vdW} + F_{H_2}^{vdW} + F_O^e + F_{H_1}^e + F_{H_2}^e - \nabla\Pi \\ &\quad + F_{hydra} + F_{app} = F_W + F_{ext}, \end{aligned} \tag{6}$$

where F_i^{vdW} and F_i^e, (where $i = O$, H_1 and H_2) denote the van der Waals forces between the i atom and the nanotube, and the electrostatic forces between the i atom and the functional group on the pore, respectively, and their values are determined by either Eqs. (2) or (3). In addition, Π, F_{hydra}, F_{app} denote the electric field generated by the charges from nearby nanotubes, the hydraulic forces in the solute and the applied force, respectively. The molecular forces comprising both the van der Waals and electrostatic forces between the water molecule and the functionalized nanotube, and external forces are given by $F_{ext} = F_{hydra} + F_{app}$. Hence, we coarse grain the external forces by the lump sum of both the hydraulic and applied forces, and the value of hydraulic forces could be obtained by either experimental data or MD simulation results. The total force between the ions and the functionalized nanotube could be deduced in a similar fashion, i.e. $F_I^{tot} = F_I + F_{ext}$, where F_I denotes the ionic forces between the ions and the functionalized nanotube. The corresponding total ionic forces between the hydrogen ion or chloride ions in the acidic solution and the functionalized nanotube are thus written as

$$F_I^{tot} = \frac{8\pi^2\eta_1\eta_2 b}{a^4\lambda^3}\left\{A\left(1+\frac{2}{\lambda}\right) - \frac{B}{5a^6\lambda^3}\left(5+\frac{80}{\lambda}+\frac{336}{\lambda^2}+\frac{512}{\lambda^3}+\frac{256}{\lambda^4}\right)\right\}$$
$$-\frac{q_I Q|Z|}{\epsilon(Z^2+b^2)^{3/2}} + F_{ext} = F_I + F_{ext}, \tag{7}$$

where $\lambda = (b^2 - a^2 + Z^2)/a^2$. For the case of the functionalized graphene sheet, the calculation is very similar to that of the nanotube, however the forms of Eqs. (2) and (3) are different due to the distinct configurations between nanotubes and graphene.

Given these force fields, the time evolution of the system can be numerically determined using the Verlet algorithm [33]

$$R_{k+1} = R_k + \tau V_k + \frac{\tau^2}{2M}F^{tot}$$
$$V_{k+1} = V_k + \frac{\tau}{M}F^{tot}, \tag{8}$$

where τ, k, M, V and F^{tot} denote the time grid size, the time step, the mass of the intruder, the velocity fields and F_W^{tot}/F_I^{tot}, respectively. To facilitate more accurate numerical outcomes, multi-step technique [34] will also be used in significant force regimes.

3 Numerical results and discussion

In this section, we carry out some numerical results derived from the theoretical frameworks given in the previous section. We consider the case of hydrogen chloride solution passing through a functionalized carbon nanotube in the first subsection, followed by the similar study for a functionalized graphene sheet in the second subsection.

3.1 Functionalized carbon nanotube

For a neutral carbon nanotube of radius 4 Å which is about the size of radius for usual (6,6) nanotube, using Eqs. (6) and (7), upon ignoring the external forces F_{ext}, the molecular forces for a water molecule and the ionic forces for a hydrogen ion permeating into the neutral nanotube are given in Fig. 3, where 400 different orientations of the water molecule are generated and the value of all relevant parameters is given in Table 1. Fig. 3 indicates that both the water molecule and the hydrogen ion could pass through the nanotube without any external forces. Moreover, the water molecule experiences stronger suck in force than that of the hydrogen ion.

Similarly, we employ Eq. (7) to determine the ionic forces for a chloride ion permeating into the neutral nanotube, which are given in Fig. 4. We note that the ionic size of the chloride ion is so large that it experiences repulsive forces near the nanotube entry, which is consistent with the results given in all theoretical investigations [10,12,14,17,24]. Therefore, without any external forces, both water molecules and hydrogen ions could spontaneously pass through the nanotube but chloride ions repeal from the nanotube. However, a peculiar effect occurs when a small positive charge,

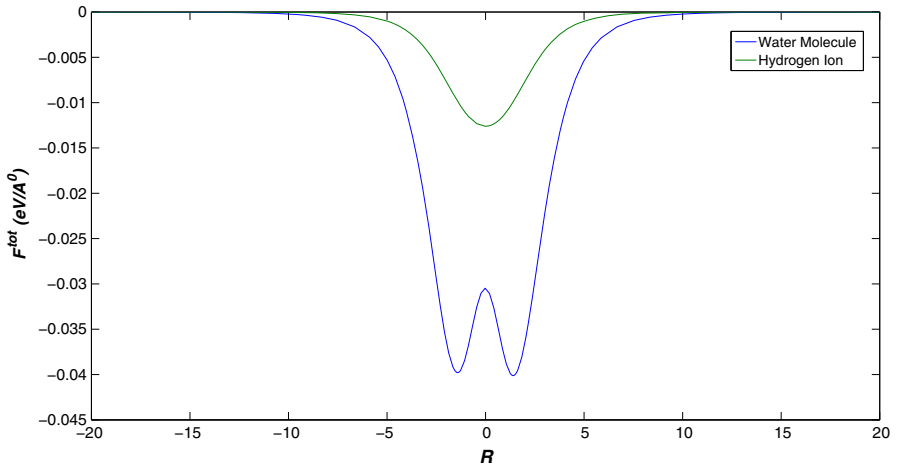

Fig. 3 Molecular forces of the water molecule and the ionic forces of hydrogen ion entering the carbon nanotube of radius 4 Å, where the negative forces imply the attractive forces generated by the nanotube. For simplicity, we adopt F^{tot} for both molecular forces F_W for water and ionic forces F_I for ions

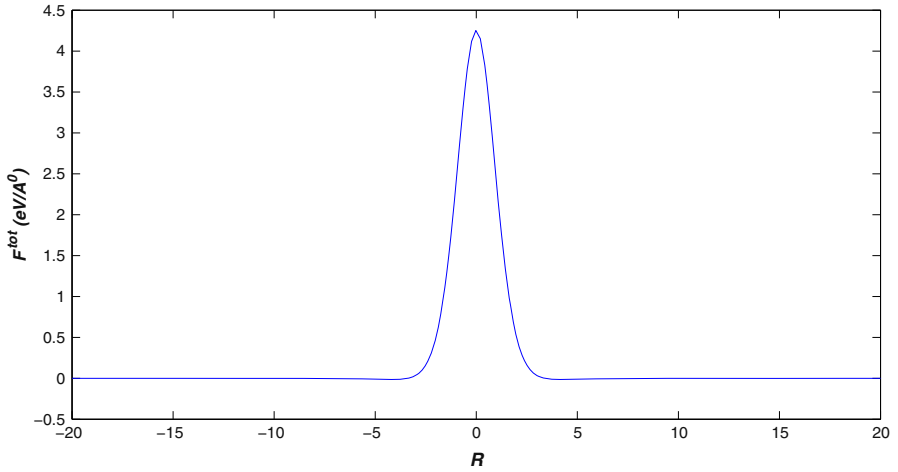

Fig. 4 Ionic forces of the chloride ion entering into the carbon nanotube of radius 4 Å

for instance $Q = 1$ e is doped on the nanotube entry. In this case, we take into account the electrostatic terms appearing in Eqs. (6) and (7) and the total molecular and ionic forces for all three intruders are plotted together in Fig. 5 for direct comparison. We observe that while the presence of the positive charges tends to shift the positive ionic forces of the chloride ion into a more negative regime, it turns the attractive forces for the water molecule and the hydrogen ion for the case of the neutral nanotube into the repulsive forces for the case of the functionalized nanotube. There exists gaps between the forces of all three intruders. However, due to the strong repulsive electrostatic interactions between the two outermost hydrogen atoms and the functional group on the

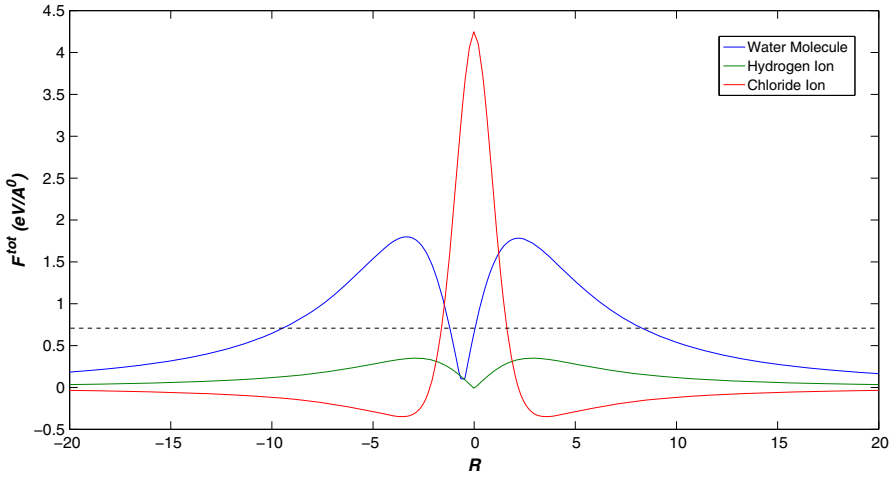

Fig. 5 Molecular forces of the water molecule and the ionic forces of hydrogen and chloride ions entering the positively charged carbon nanotube of doped charge 1e

nanotube's vicinity, the repulsive forces of the water molecule are stronger than that of the hydrogen ion. There must exists certain F_{ext} comprising both the hydraulic and applied forces as indicated by the dash horizontal line in Fig. 5 such that only hydrogen ions could pass through the functionalized nanotube leaving both water and chloride ions on the feed side. Mathematically, F_{ext} could be determined by the consideration of energy conservation, which is given by

$$\int_0^{R_0} F_W dR > \int_0^{R_0} F_{ext} dR > \int_0^{R_0} F_H dR, \tag{9}$$

where R_0, F_H and F_W denote the initial axial position of the intruder, the ionic forces of the hydrogen ion and the molecular forces of the water molecule, respectively.

3.2 Functionalized graphene sheet

Now we turn our attention into the similar problem using functionalized graphene sheet. Due to the fact that the ionic size of chloride ion is larger than the pore size of the graphene sheet, chloride ions are always blocked by the graphene. We again employ Eqs. (6) and (7) but in analogous forms taking into account of the geometric configuration for the graphene sheet to determine the molecular and ionic forces of the water molecule and the hydrogen ion permeating into the neutral graphene. In this case, only semi-analytical forms are feasible for all single and double surface integrals. Due to the small pore size of the graphene sheet, both the water molecule and the hydrogen ion experience repulsive forces on the pore entry, which are shown in Figs. 6 and 7, respectively, where 100 different orientations for the water molecule are generated. For the neutral graphene, since the repulsive forces for the water molecule are stronger than that of the hydrogen ion, Eq. (9) is automatically satisfied. However

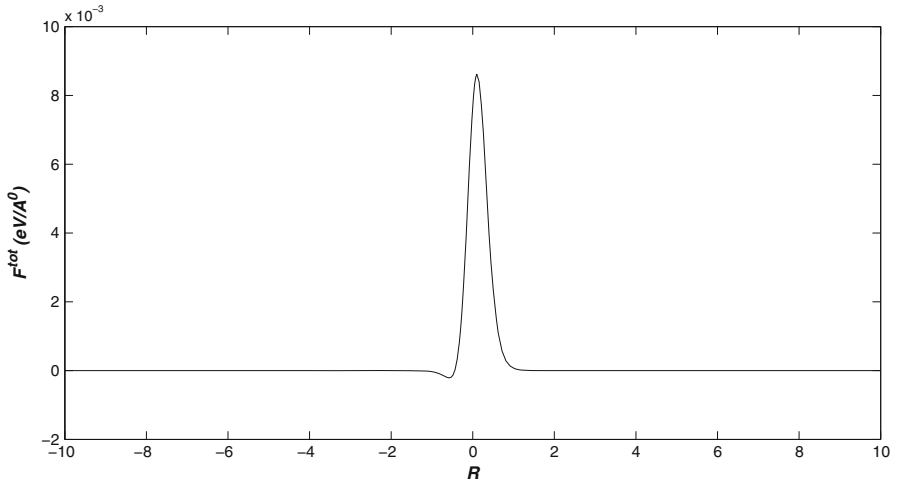

Fig. 6 Molecular forces of the water molecule permeating into a neutral graphene sheet

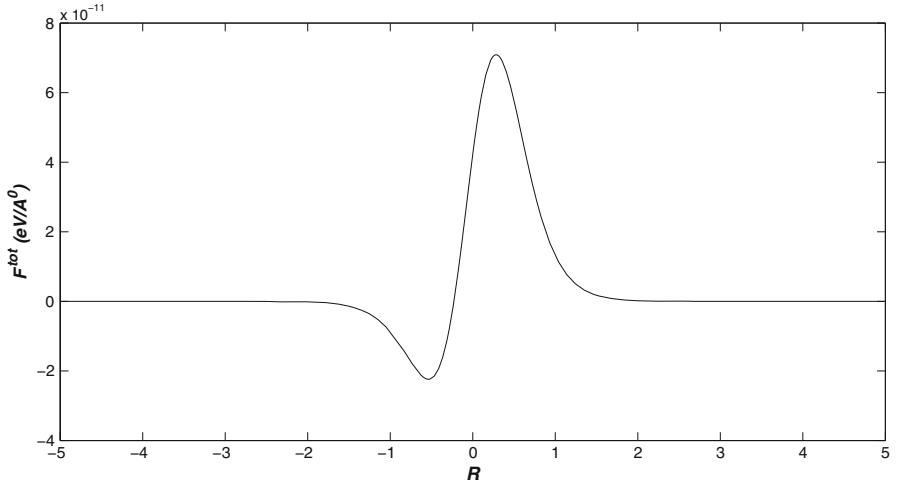

Fig. 7 Ionic forces of the hydrogen ion permeating into a neutral graphene sheet

the gap between both repulsive forces is so narrow that it poses a technical difficulty to extract hydrogen ions using the mean of reverse osmosis, especially when the thermal fluctuation is considered.

To tackle this problem, again we dope some positive charges, for instance $Q = 0.5$ e around the pore of the graphene. In this case, the electrostatics interactions arising between the water molecule or the hydrogen ion and the functional group are incorporated into both the molecular and ionic forces, and the numerical results are shown in Fig. 8. We again observe that due to the stronger interactions between the two outermost hydrogen atoms on the surface of water molecule and the functional group, the repulsive forces for the water molecule are much stronger than that of the

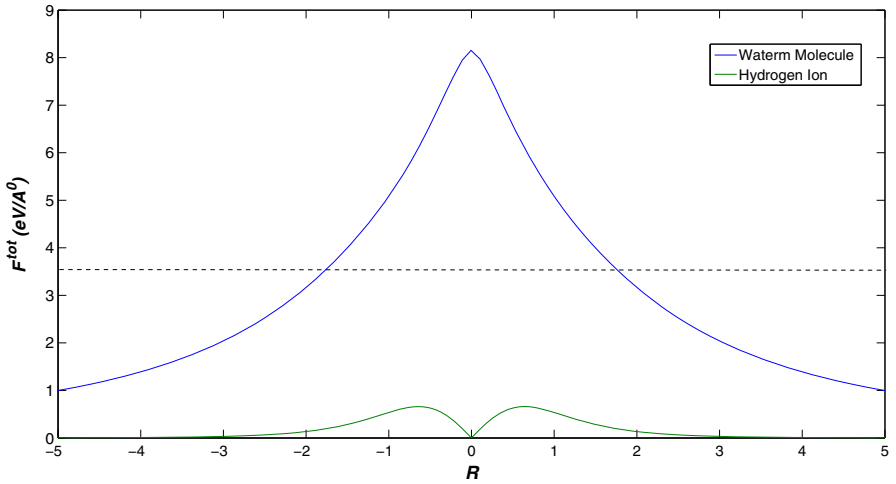

Fig. 8 Molecular forces of the water molecule and the ionic forces of hydrogen ion entering the graphene-oxide of charge 0.5 e

hydrogen ion. Equation (9) could then be employed to determine the external forces F_{ext} for the realization of the hydrogen yield.

To visually demonstrate such effect, we illustrate a dynamic evolution of the water molecule and the hydrogen ion permeating into the functionalized graphene sheet by incorporating the corresponding force fields into the Verlet algorithm given by Eq. (8). For simplicity, we assume a hydraulic forces, i.e 0.005 eV/Å which fade out exponentially towards the functionalized graphene and the applied force of 0.1 eV/Å which satisfies Eq. (9). From Fig. 8, since most significant ionic interactions for the hydrogen ion occur within 1 Å apart from the pore center, multi-step technique with the refinement of 5 is employed to cultivate more accurate numerical results. The numerical results for the initial position $R_0 = 10$ Å are given in Fig. 9. We observe that both the water molecule and the hydrogen ion are initially driven by the applied force toward the functionalized graphene. However, near the pore entry, water molecule does not gain enough work to overcome the energy barrier induced by the pore vicinity and rebounds, while the hydrogen ion could pass through the pore into the permeate side. The outcome of the entire revise osmosis results in sole hydrogen ions on the permeate side. Finally, hydrogen could be produced by a chemical reduction which simply replaces a key component in the latest biological way of producing hydrogen using photosynthetic microorganisms and biomass [35,36], where photosynthesis splits water into hydrogen ions (H^+) and electrons (e^-), and these hydrogen ions could be collected and combined into hydrogen gas by a chemical reduction, i.e. $2H^+ + 2e^{-1} \rightarrow H_2$ using special enzymes [35–37].

Although both the functionalized carbon nanotube and graphene sheet could achieve the similar outcomes. However, due to the negligible thickness of graphene sheet and the larger energy gap between the hydrogen ion and the water molecule, functionalized graphene turns out to be the better material for the current purpose. The merits of present methodology over other more complicated MD simulations are that we could

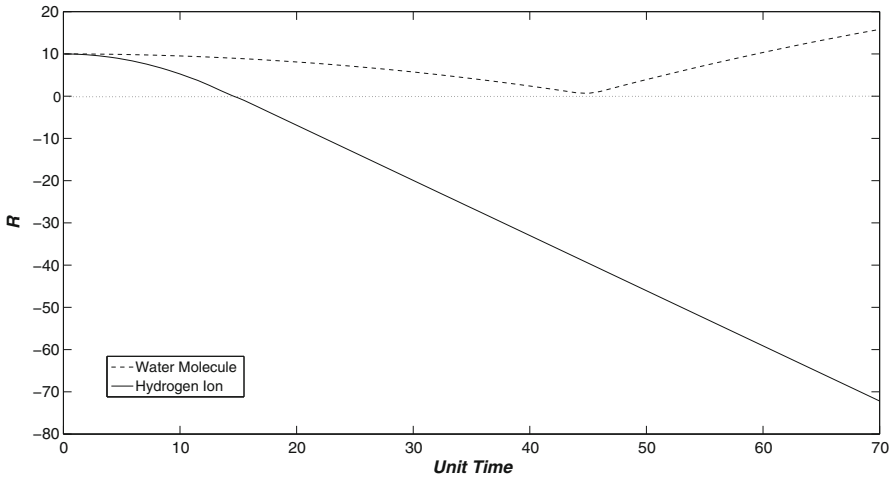

Fig. 9 MD simulations of water molecule and hydrogen ion permeating into a positive charged graphene-oxide, where hydrogen ion passes through the functionalized graphene leaving both water and chloride ions on the feed side

obtain numerical solutions almost instantaneously using normal PCs and deductive results which could be deduced by simply varying parameters such as temperatures and pressures appearing in the analytical/semi-analytical formulae.

4 Conclusion

In this paper, we adopt both the continuous approximation and MD simulations to investigate the hydrogen yield using the functionalized carbon nanotubes and graphene sheets. We show that both materials could achieve the same goal due to the existence of a gap between the repulsive forces for both the water molecule and the hydrogen ion. However, due to the larger gap for the repulsive forces and the negligible thickness of the functionalized graphene sheet, graphene turns out to be the better candidate for the current purpose. This phenomenon could only happen when the repulsive forces for the water molecule induced by a nanomaterial is larger than that of the hydrogen ion, and the external forces F_{ext} satisfy the inequality given in Eq. (9). Least but not last, the validity of the paper is subject to further experimental and computational outcomes.

Acknowledgments We gratefully acknowledge the financial support from the International Conference Grant and Small Research Grant from UNNC, Ningbo Natural Science Foundation (2014A610025) and (2014A610172), and Qianjiang Talent Scheme (QJD1402009).

References

1. A. Demirbas, Gaseous products from biomass by pyrolysis and gasification: effects of catalyst on hydrogen yield. Energy. Convers. Manag. **43**, 897–909 (2002)

2. Y.H.P. Zhang, B.R. Evans, J.R. Mielenz, R.C. Hopkins, M.W.W. Adams, High-yield hydrogen production from starch and water by a synthestic enzymatic pathway. PLOSOne **e456**, 1–6 (2007)
3. Y. Tao, Y. Chen, Y. Wu, Y. He, Z. Zhou, High hydrogen yield from a two-step process of dark-and photo-fermentation of sucrose. Int. J. Hydrog. Energy **32**, 200–206 (2007)
4. T. De Vrije, A.E. Mars, M.A.W. Budde, M.H. Lai, C. Dijkema, P. De Waard, P.A.M. Claassen, Glycolytic pathway and hydrogen yield studies of the extreme thermophile caldicellulosiruptor saccharolyticus. Appl. Microbiol. Biotechnol. **74**, 1358–1367 (2007)
5. H. Argun, F. Kargi, I. Kapdan, R. Oztekin, Biohydrogen production by dark fermentation of wheat powder solution: effects of C/N and C/P ratio on hydrogen yield and formation rate. Int. J. Hydrog. Energy **33**, 1813–1819 (2008)
6. N. Kumar, D. Das, Enhancement of hydrogen production by enterobacter cloacae IIT-BT08. Process Biochem. **35**, 589–593 (2000)
7. H. Yu, Z. Zhu, W. Hu, H. Zhang, Hydrogen production from rice winery wastewater in an upflow. Int. J. Hydrog. Energy **27**, 1359–1365 (2002)
8. T. Nakamura, Hydrogen production from water utilizing solar heat at high temperature. Solar Energy **19**, 467–475 (1977)
9. Y. Chan, J.M. Hill, A mechanical model for single-file transport of water through carbon nanotube membranes. J. Membr. Sci. **372**, 57–65 (2011)
10. Y. Chan, J.M. Hill, Modeling on ion rejection using membranes comprising ultra-small radii carbon nanotubes. Eur. Phys. J. B. **85**, 56 (2012)
11. Y. Chan, J.M. Hill, Ion selectivity using membranes comprising functionalized carbon nanotubes. J. Math. Chem. **51**, 1258–1273 (2013)
12. Y. Chan, Mathematical modeling on ultra-filtration using functionalized carbon nanotubes. Appl. Mech. Mater. **51**, 1258–1273 (2013)
13. K. Severin, Boronic acids as building blocks for molecular nanstructures and polymeric materials. Dalton Trans. **27**, 5254–5264 (2009)
14. T. Hilder, D. Gordon, S. Chung, Salt rejection and water transport through boron nitride nanotubes. Small **5**, 2183–2190 (2009)
15. S. Joseph, R.J. Mashl, E. Jakobasson, N.R. Aluru, A new water phase induced by confinement in nanotubes. Nature **3**, 13991403 (2003)
16. G. Hummer, J.C. Rasaiah, J.P. Noworyta, Water conduction through the hydrophobic channel of a carbon nanotube. Nature **414**, 188–190 (2001)
17. B. Corry, Designing carbon nanotube membranes for efficient water desalination. J. Phys. Chem. B **112**, 1427–1434 (2008)
18. C. Song, B. Corry, Intrinsic ion selectivity of narrow hydrophobic pores. J. Phys. Chem. B **113**, 7642–7649 (2009)
19. A. Berezhkovskii, G. Hummer, Single-file transport of water molecules through a carbon nanotube. Phys. Rev. Lett. **89**, 064503 (2002)
20. G. Zuo, R. Shen, S. Ma, W. Guo, Transport properties of single-file water molecules inside a carbon nanotube biomimicking water channel. ACS Nano **4**, 205–210 (2010)
21. A. Kalra, S. Garde, G. Hummer, Osmotic water transport through carbon nanotube membranes. PNAS **100**, 10175–10180 (2003)
22. M.S.P. Sansom, I.H. Shrivastava, K.M. Ranatunga, G.R. Smith, Simulations of ion channels watching ions and water move. Trends Biochem. Sci. **25**, 368–374 (2000)
23. M. Theresa, M. Pendergast, E.M.V. Hoek, A review of water treatment membrane nanotechnologies. Energy Environ. Sci. **4**, 1946–1971 (2011)
24. D.C. Tanugi, J.C. Grossman, Water desalination across nanoporous graphene. Nano Lett. **12**, 3602–3608 (2012)
25. J.Y. Choi, Graphene transfer: a stamp for all substrates. Nature **8**, 311–312 (2013)
26. B.J. Cox, N. Thamwattana, J.M. Hill, Mechanics of atoms and fullerenes in single-walled carbon nanotubes. I. Acceptance and suction energies. Proc. R. Soc. Lond. Ser. A **463**, 461 (2007)
27. B.J. Cox, N. Thamwattana, J.M. Hill, Mechanics of atoms and fullerenes in single-walled carbon nanotubes. II. Oscillatory behaviour. Proc. R. Soc. Lond. Ser. A **463**, 477 (2007)
28. Y. Chan, *Modelling and md simulations on ultra-filtration using graphene sheet*. (submitted to IEEE NANO for publication) (2014)

29. D. Baowan, K. Chayantrakom, P. Satiracoo, B.J. Cox, Mathematical modelling for equilibrium configurations of concentric gold nanoparticles as potential application in drug and gene delivery. J. Math. Chem. **49**, 1042–1053 (2011)
30. K. Sumetpipat, R.K.F. Lee, B.J. Cox, J.M. Hill, D. Baowan, Carbon nanotori and nanotubes encapsulating carbon atomic-chains. J. Math. Chem. **52**, 1817–1830 (2014)
31. J.E. Jones, On the determination of molecular fileds. I. From the variation of the viscosity of a gas with temperature. Proc. R. Soc. **106A**, 441 (1924)
32. M. Sprik, M.L. Klein, K. Watanabe, Solvent polarization and hydration of the chlorine anion. J. Phys. Chem. **94**, 6483–6488 (1990)
33. T. Pang, *An Introduction to Computational Physics* (Cambridge University Press, Cambridge, 2006)
34. E. Weinan, *Principles of Multiscale Modeling* (Cambridge University Press, Cambridge, 2011)
35. M. Ni, D.Y.C. Leung, M.K.H. Leung, K. Sumathy, An overview of hydrogen production from biomass. Fuel Process. Technol. **87**, 461–472 (2006)
36. A. Volgusheva, S. Styring, F. Mamedov, Increased photosystem ii stability promotes h_2 production in sulfur-deprived chlamydomonas reinhardtii. PNAS **110**, 7223–7228 (2012)
37. Y.Z. Voloshin, A.V. Dolganov, O.A. Varzatskii, Y.N. Bubnov, Efficient electrocatalytic hydrogen production from h^+ ions using specially designed boron-capped cobalt clathrochelates. Chem. Commun. **47**, 7737–7739 (2011)
38. G.C. Maitland, M. Rigby, E.B. Smith, W.A. Wakeham, *Intermolecular Forces: Their Origin and Determination* (Clarendon Press, Oxford, 1981)